

A Simple Mass-Spring Model With Roller Feet Can Induce the Ground Reactions Observed in Human Walking

Ben R. Whittington

Department of Mechanical Engineering,
University of Wisconsin–Madison,
Madison, WI 53706

Darryl G. Thelen

Department of Mechanical Engineering,
Department of Biomedical Engineering,
and Department of Orthopedics and
Rehabilitation,
University of Wisconsin–Madison,
Madison, WI 53706
e-mail: thelen@engr.wisc.edu

It has previously been shown that a bipedal model consisting of a point mass supported by spring limbs can be tuned to simulate periodic human walking. In this study, we incorporated roller feet into the spring-mass model and evaluated the effect of roller radius, impact angle, and limb stiffness on spatiotemporal gait characteristics, ground reactions, and center-of-pressure excursions. We also evaluated the potential of the improved model to predict speed-dependent changes in ground reaction forces and center-of-pressure excursions observed during normal human walking. We were able to find limit cycles that exhibited gait-like motion across a wide spectrum of model parameters. Incorporation of the roller foot ($R = 0.3$ m) reduced the magnitude of peak ground reaction forces and allowed for forward center-of-pressure progression, making the model more consistent with human walking. At a fixed walking speed, increasing the limb impact angle reduced the cadence and prolonged stance duration. Increases in either limb stiffness or impact angle tended to result in more oscillatory vertical ground reactions. Simultaneous modulation of the limb impact angle and limb stiffness was needed to induce speed-related changes in ground reactions that were consistent with those measured during normal human walking, with better quantitative agreement achieved at slower speeds. We conclude that a simple mass-spring model with roller feet can well describe ground reaction forces, and hence center of mass motion, observed during normal human walking. [DOI: 10.1115/1.3005147]

Keywords: gait, dynamic simulation, limit cycle, limb stiffness

Introduction

Simple models of human walking have provided tremendous insights into the mechanics of gait, benefiting from the idea that “simplicity promotes understanding” [1]. The classic model of gait is an inverted pendulum, which is useful in describing the exchange between gravitational potential and kinetic energies during single support [2]. Compass models, consisting of two coupled inverted pendulums, can achieve stable limit cycles when walking down a slight ($\sim 3\%$) slope, demonstrating that passive dynamical properties lead naturally to bipedal walking patterns [1,3]. Simple ankle push-off actuation can be used to efficiently power a compass model on level ground [4], with the energetic requirements at varying speeds mimicking that seen in humans [5]. Further, the incorporation of roller feet on the inverted pendulum-type limbs [6] can account for the progression of the center of pressure (COP) under the human foot during stance [7]. While providing many important insights, it has long been recognized that inverted pendulum models are not good predictors of the ground reaction forces, and hence center of mass (COM) motion, throughout a normal gait cycle [8,9].

A recent study showed that a bipedal mass-spring model, which has classically been used to describe running [10], can also be tuned to reproduce the characteristic vertical and anterior-posterior (A-P) ground reaction forces observed during human walking [11]. However, the classic spring-mass model [10,12] has a point foot and therefore a fixed COP during stance. In contrast, a roller foot would allow for the COP to progress, thereby reduc-

ing the horizontal distance between the COP and COM. Such an effect could potentially induce a more vertically oriented ground reaction force and hence smaller breaking and push-off forces during early and late phases of stance.

In this study, we developed and used a mass-spring model with roller feet to simulate human walking. The following three purposes were addressed with the model. First, we determined the effect of the roller foot on the ground reactions and COP excursions seen during stance. We hypothesized that increasing the roller foot radius would reduce A-P force magnitudes while inducing center-of-pressure excursions that are more consistent with human gait. Our second purpose was to evaluate the effect of roller radius, limb impact angle, and limb stiffness on cadence, step length, walking speed, and induced ground reactions. The third purpose was to determine if modulation of limb stiffness and impact angle is sufficient to induce the speed-dependent changes in cadence, step length, ground reactions, and center-of-pressure excursions seen in normal human walking.

Methods

The model consisted of a point mass (M), two massless limb springs of stiffness K , and massless circular roller feet of radius R (Fig. 1). The base of each limb spring was rigidly fixed to its roller foot, such that a single angle (θ) defined the orientation of a limb and a foot with respect to a vertical upright. The proximal end of the limb spring was pinned to the point mass. Thus, the configuration of each limb was described by a limb angle θ and spring length L .

Equations of motion (Eq. (1)) for the model were derived in terms of the trailing limb (denoted by subscript 1) using a Lagrangian approach (Appendix A),

Contributed by the Bioengineering Division of ASME for publication in the JOURNAL OF BIOMECHANICAL ENGINEERING. Manuscript received July 27, 2007; final manuscript received June 17, 2008; published online November 26, 2008. Review conducted by Yener N. Yeni.

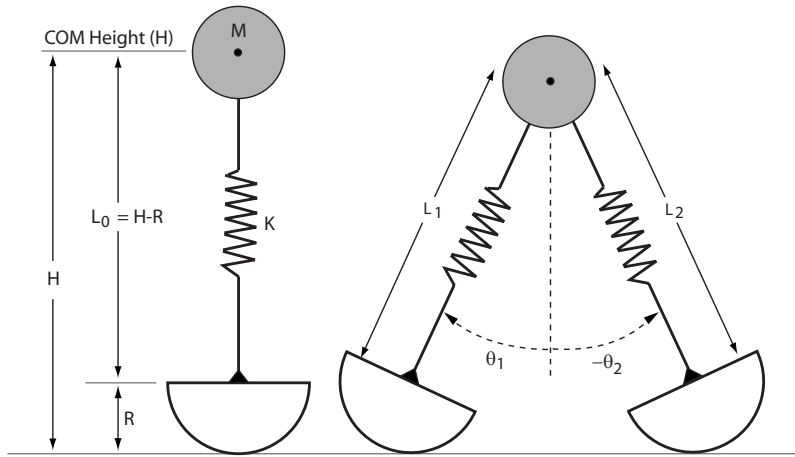


Fig. 1 Each limb was represented by a translational spring, with stiffness K and slack length L_0 , that was rigidly coupled to a roller of radius R on one side and pinned to a point mass M on the other side. The point mass was assumed to be at the height H of the center of mass of the body with the limb spring in an unstretched upright configuration. Simulations were performed assuming normative values of $H=1$ m and $M=80$ kg. Roller radii of 0.0 m, 0.1 m, 0.2 m, 0.3 m, and 0.4 m were considered.

$$\begin{bmatrix} MR \sin \theta_1 & M \\ ML_1^2 + 2ML_1R \cos \theta_1 + MR^2 & MR \sin \theta_1 \end{bmatrix} \begin{pmatrix} \ddot{\theta}_1 \\ \ddot{L}_1 \end{pmatrix} = \begin{bmatrix} -MR\dot{\theta}_1^2 \cos \theta_1 + ML_1\dot{\theta}_1^2 + M\dot{\theta}_1^2R \cos \theta_1 - Mg \cos \theta_1 \\ + KL_0 - KL_1 + (KL_0 - KL_2) \left(\frac{L_2 \cos(\theta_1 - \theta_2) + R \cos \theta_1}{L_2 + R \cos \theta_2} \right) \\ -2ML_1\dot{L}_1\dot{\theta}_1 - 3M\dot{L}_1\dot{\theta}_1R \cos \theta_1 + ML_1\dot{\theta}_1^2R \sin \theta_1 + M\dot{L}_1R\dot{\theta}_1 \cos \theta_1 + MgL_1 \sin \theta_1 \\ + (KL_0 - KL_2) \left(\frac{RL_2 \sin \theta_2 - L_1L_2 \sin(\theta_1 - \theta_2) - RL_1 \sin \theta_1}{L_2 + R \cos \theta_2} \right) \end{bmatrix} \quad (1)$$

where g represents the gravitational acceleration and L_0 represents the spring slack length.

For each simulation, the model was initially positioned in upright single support with the point mass at its apex and the swing limb positioned out in front of the stance limb at a prescribed impact angle (Fig. 2). During the initial single support period, the equations of motion (Eq. (1)) were numerically integrated forward in time until contact of the leading limb with the ground was detected. We

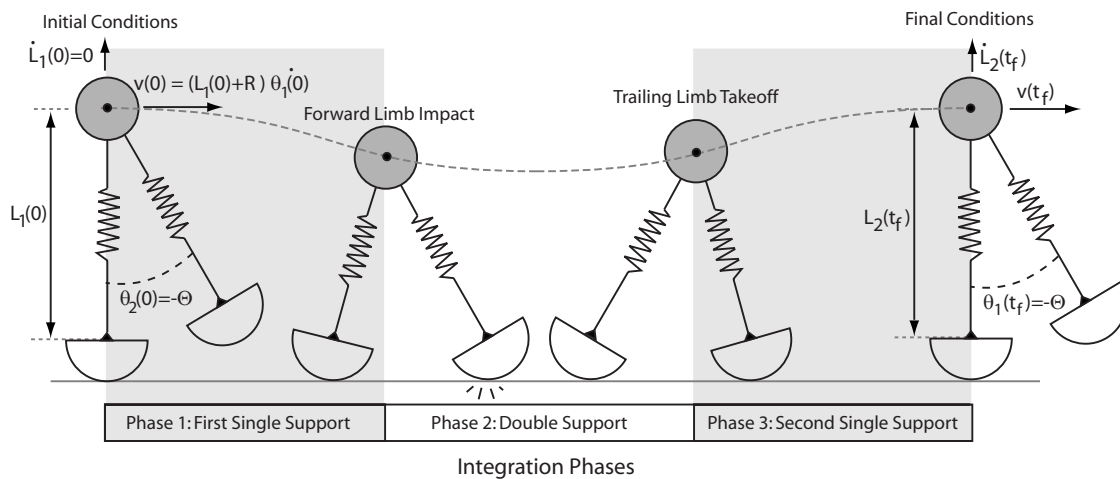


Fig. 2 Simulations were started with the trailing limb in an upright configuration and the forward limb oriented at the impact angle. The double support phase started when the leading limb contacted the ground and then continued until the trailing limb length reached its undeflected length. The second single support phase continued until the limb reached an upright configuration, signaling the end of the half gait cycle. We searched for limit cycle solutions in which the limb length, forward velocity, and vertical velocity at the end of the half gait cycle replicated the initial conditions.

assumed that there was no slip between either of the rollers and ground during contact. As a result, during double support, the closed loop kinematic constraints could be used to determine the forward limb spring velocity and rotational angular velocity (denoted by limb 2) as a function of the trailing limb states,

$$\begin{Bmatrix} \dot{L}_2 \\ \dot{\theta}_2 \end{Bmatrix} = \begin{bmatrix} \frac{L_2 \cos(\theta_1 - \theta_2) + R \cos \theta_1}{L_2 + R \cos \theta_2} & \frac{RL_2 \sin \theta_2 - L_1 L_2 \sin(\theta_1 - \theta_2) - RL_1 \sin \theta_1}{L_2 + R \cos \theta_2} \\ \frac{\sin(\theta_1 - \theta_2)}{L_2 + R \cos \theta_2} & \frac{R \cos \theta_2 + L_1 \cos(\theta_1 - \theta_2)}{L_2 + R \cos \theta_2} \end{bmatrix} \begin{Bmatrix} \dot{L}_1 \\ \dot{\theta}_1 \end{Bmatrix} \quad (2)$$

Differentiation of Eq. (2) resulted in the following relationship (Eq. (3)) between the accelerations of the leading and trailing limbs during double support:

$$\begin{Bmatrix} \ddot{L}_2 \\ \ddot{\theta}_2 \end{Bmatrix} = \begin{bmatrix} \frac{L_2 \dot{\theta}_1 (L_2 \dot{\theta}_2 \cos(\theta_1 - \theta_2) - \dot{L}_2 \sin(\theta_1 - \theta_2))}{\dot{\theta}_2^2} & \frac{-L_2 (L_2 \dot{\theta}_2 L_1 \dot{\theta}_1 \sin(\theta_1 - \theta_2) - L_2 \dot{\theta}_2 \dot{L}_1 \cos(\theta_1 - \theta_2) + \dot{L}_2 L_1 \dot{\theta}_1 \cos(\theta_1 - \theta_2) + \dot{L}_2 \dot{L}_1 \sin(\theta_1 - \theta_2))}{\dot{\theta}_2^2} \\ \frac{\dot{\theta}_1 \dot{\theta}_2 \sin(\theta_1 - \theta_2)}{L_2} & \frac{\dot{\theta}_2 (L_1 \dot{\theta}_1 \cos(\theta_1 - \theta_2) + \dot{L}_1 \sin(\theta_1 - \theta_2))}{L_2} \end{bmatrix} \times \begin{Bmatrix} \ddot{L}_1 \\ \ddot{\theta}_1 \end{Bmatrix} \quad (3)$$

Double support continued until the trailing limb spring reached its slack length. At this point, the trailing limb was then reset in front of the body at the limb impact angle (Fig. 2). This swing limb motion incurred no energetic cost since the limb and foot were assumed massless. Numerical integration continued into the subsequent single limb support phase until the leading limb reached an upright configuration, and the half cycle of gait was complete. Throughout this process, integration was stopped in the case of circumstances not representative of gait (i.e., take-off in single limb support, falling backward, or the mass bottoming out). The total system energy (TE) for the conservative system was calculated by summing kinetic, spring potential, and gravitational potential energies,

$$TE = \frac{1}{2} M |\vec{v}|^2 + \frac{1}{2} K (L_0 - L_1)^2 + \frac{1}{2} K (L_0 - L_2)^2 + Mg(R + L_i \cos \theta_i) \quad (4)$$

(kinetic) (spring potential) (gravitational potential)

where \vec{v} is the velocity of the point mass (Eq. (A2), Appendix), and L_i and θ_i refer to a limb currently in contact.

Given a set of model parameters and desired walking speed, a nonlinear equation solver (fsolve, MATLAB®) was used to determine a set of initial states such that a limit cycle behavior was achieved. Specifically, we solved for initial states of the trailing limb ($L_1(0), \dot{\theta}_1(0)$) such that the states of the second limb at the end of the half gait cycle matched the initial states of the first stance limb ($\dot{\theta}_2(t_f) = \dot{\theta}_1(0), L_2(t_f) = L_1(0)$) while also achieving the desired average walking speed. The limb spring velocity in the initial upright configuration was assumed to be zero for all simulations (i.e., $\dot{L}_1(0) = 0$). We evaluated the effect of limb stiffness (K), roller radius ($R = 0.0$ m, 0.1 m, 0.2 m, 0.3 m, and 0.4 m), and limb impact angle Θ on the limit cycle behavior at slow (1.06 m/s), preferred (1.35 m/s), and fast (1.59 m/s) walking speeds. The excursion of the center of pressure during stance was quantified by tracking the contact point of the roller foot with the ground. Ground reaction forces in the A-P and vertical directions could then be computed at each time step using the roller contact point, the spring deflection, and the point mass location (Appendix B). Graphical representations of the solutions were used to evaluate the effects of model parameters on step length, cadence, total energy, COP excursions, and ground reactions at parameter combinations where limit cycle solutions were found.

Comparison With Experimental Gait Data. Gait analysis was conducted on 20 healthy young subjects including 9 males

(age of 24 ± 4 , height of 182 ± 10 cm, and mass of 79 ± 8 kg) and 11 females (age of 24 ± 3 , height of 166 ± 10 cm, and mass of 58 ± 13 kg). Subjects had no history of major orthopedic diagnosis, musculoskeletal trauma, or persistent joint pain. Each subject gave informed consent according to a protocol approved by the University of Wisconsin's Health Sciences Institutional Review Board. Subjects walked at three speeds (80%, 100%, and 120% of preferred) while their motion was tracked using a passive motion capture system and ground reaction forces were recorded at 2000 Hz from three imbedded force plates. Ground reaction data were used to identify heel contact and toe-off times. Ground reaction forces were then normalized to body mass and ensemble averaged across subjects to obtain a representative set of ground reaction force curves for each of the walking speeds. Similarly, measured COP excursions were averaged to generate representative excursions for all three walking speeds. Spatiotemporal gait variables (stride length, gait speed, and cadence) were subsequently calculated from the measured kinematic data and compared to simulation results.

We generated simulations of a half gait cycle that were able to best replicate the ground reactions measured experimentally. This was done by first establishing regions within the solution space that led to simulations that were within one standard deviation of the cadence and step length measured experimentally at each speed. We then determined which parameter combinations within these regions induced ground reaction forces that best matched the average experimental forces. We used the sum of squared differences between the simulated and experimental ground reaction forces, normalized to the standard deviation of the experimental data, as the measure of goodness of fit.

Results

At each walking speed, a large array of limit cycle solutions was found in which the system state at the end of a half gait cycle replicated the initial conditions at the start of the half gait cycle. Thus, each solution represented a periodic gait cycle during which constant total energy was maintained, while energy transfer occurred between gravitational potential energy, elastic potential energy, and kinetic energy (Fig. 3).

Roller radius effect. As hypothesized, increasing the roller radius (while leaving other parameters constant) resulted in a decrease in both the peak vertical and A-P ground reactions at a fixed walking speed (Fig. 4). Increasing the roller radius also resulted in greater COP excursion, with the change in excursion

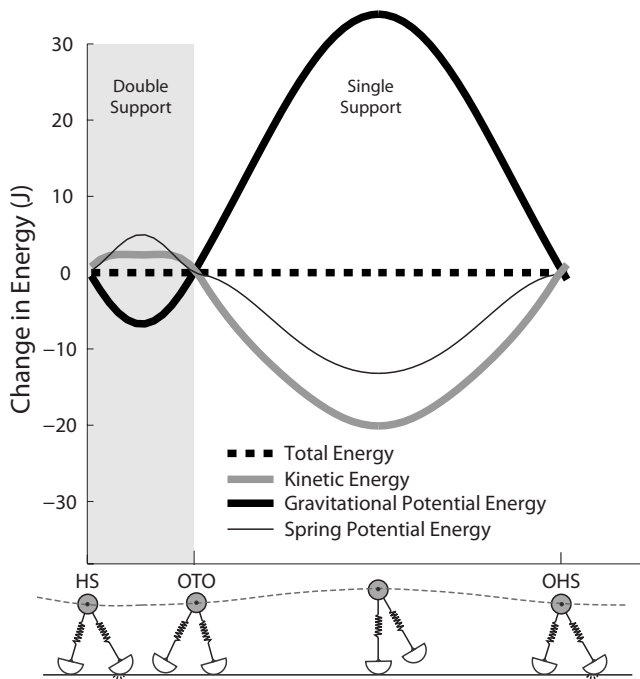


Fig. 3 The simple mass-spring model of walking is conservative, such that there was no change in total energy across a half gait cycle. The increase in gravitational potential energy during the first half of single support occurs as a result of both limb spring lengthening (decrease in spring potential energy) and a reduction in forward velocity (decrease in kinetic energy). A 0.3 m radius roller was used to generate this 1.35 m/s walking speed simulation. Abbreviations: HS—heel strike, OTO—opposite toe-off, and OHS—opposite heel strike.

increasing approximately linearly with the radius of the roller.

Stiffness and impact angle effects. With a fixed roller radius, the model was capable of walking at a fixed speed with different combinations of limb stiffness and impact angle (Fig. 5). Each solution corresponded to a specific step length (Fig. 5(a)), cadence (Fig. 5(b)), and total energy state (Fig. 5(c)). Increasing the limb impact angle resulted in longer step lengths, a reduction in cadence, and a decrease in total energy. Varying the limb stiffness had a smaller effect on the step length and cadence but had a large

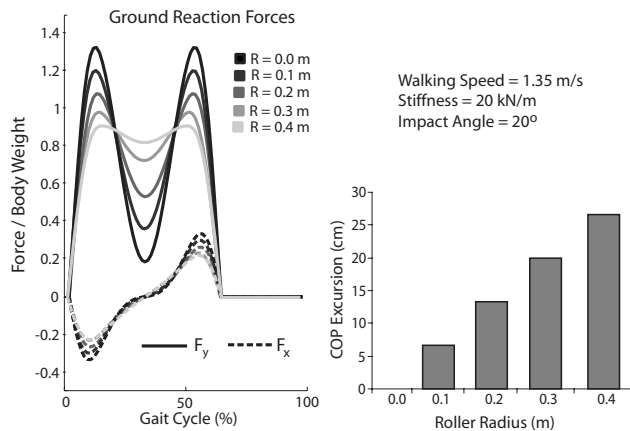


Fig. 4 Inclusion of a roller in the mass-spring model decreased the magnitude of the peak ground reaction forces in both the anterior (F_x) and vertical (F_y) directions. The forward progression of the center of pressure, as measured by the COP excursion during stance, increased approximately linearly with the radius of the roller.

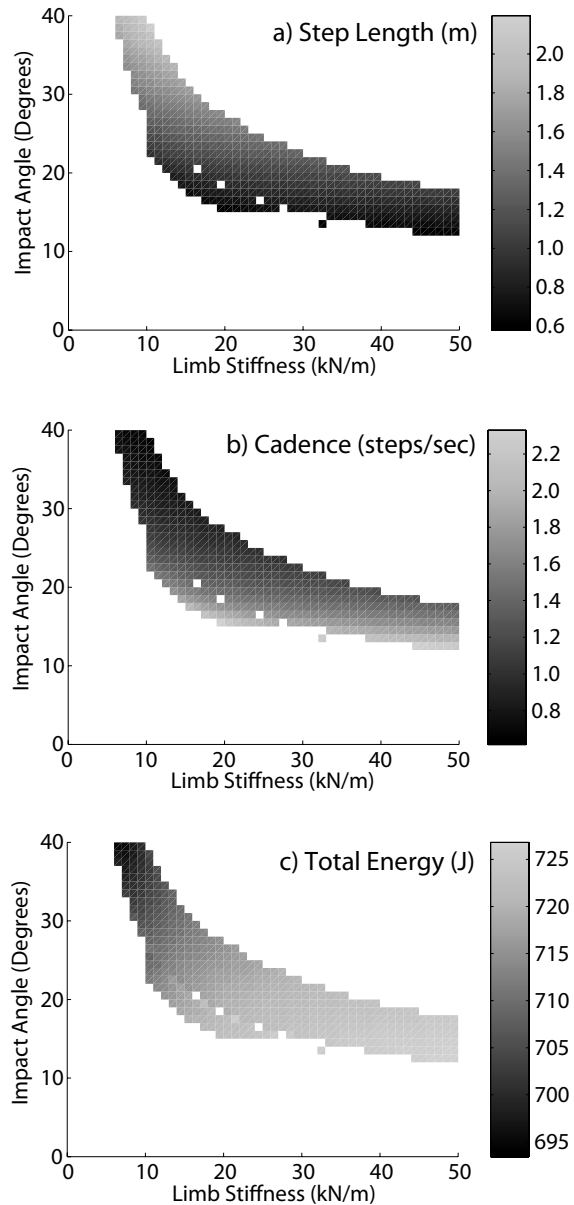


Fig. 5 Shown are the limb stiffness and impact angles that resulted in limit cycle solutions when the 0.3 m roller radius model walked with an average velocity of 1.35 m/s. Each solution exhibits specific (a) step length, (b) cadence, and (c) total energy. The highest energy states were associated with high cadence–low step length solutions, achieved via coupling high limb stiffness with small impact angles.

effect on total energy, with a stiffer limb resulting in an increase in energy.

Variations in the impact angle and limb stiffness both had a substantial effect on the duration and magnitude of the ground reactions. An increase in impact angle at a constant stiffness resulted in a substantial increase in peak anterior-posterior and vertical ground reaction forces and a longer stance period (Fig. 6). An increase in limb stiffness at a constant impact angle also acted to increase the peak A-P and vertical ground reactions, with the effect being slightly more pronounced at larger impact angles.

Using a fixed roller radius of 0.3 m, limit cycle solutions were found that were able to closely emulate the COP progression exhibited by the subjects at the slow, preferred and fast speeds (Fig. 7). Simultaneous increases in both the limb impact angle and limb stiffness resulted in the best agreement of the model predictions

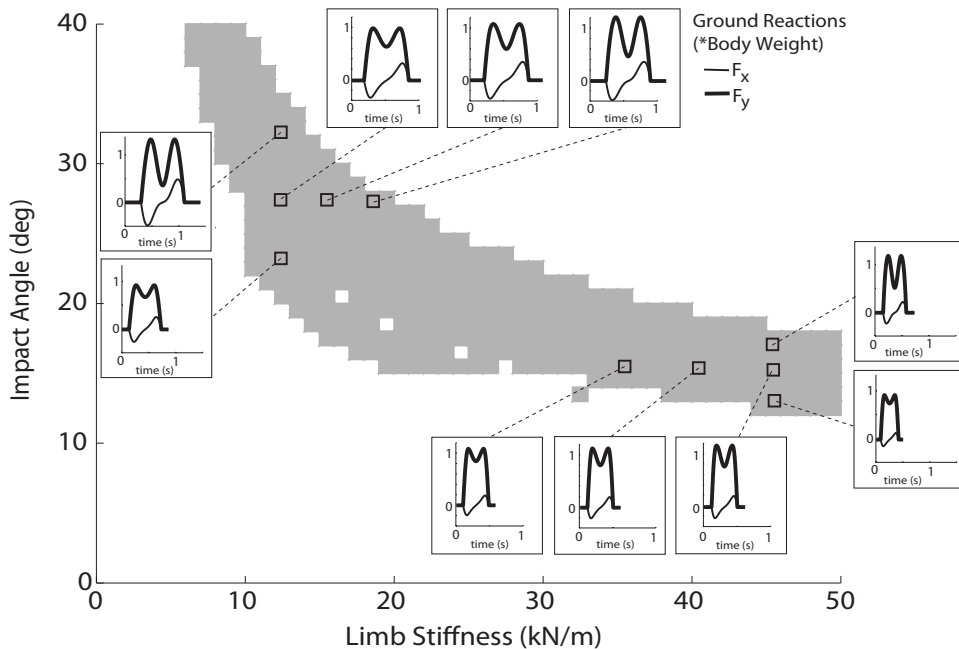


Fig. 6 Variations in limb stiffness and impact angle altered the ground reactions that were induced when walking with a 0.3 m radius roller at an average velocity of 1.35 m/s. An increase in impact angle resulted in larger peak ground reaction forces in both the anterior (F_x) and vertical (F_y) directions and also substantially prolonged the stance period. Increasing limb stiffness tended to induce slightly larger vertical ground reactions.

with the speed-related changes in ground reactions (Table 1). The smallest quantitative differences with average ground reactions were achieved at a slow walking speed (Fig. 7), with root mean squared (rms) differences of 2.8% and 6.7% body weights in the horizontal and vertical directions, respectively. At faster speeds, the simulated vertical force tended to exhibit greater oscillation during stance than that observed experimentally (Fig. 7). In addition, simulations at all three speeds predict a greater braking force on the leading limb during the early stance than is observed experimentally.

Discussion

This study demonstrates that a simple bipedal spring-mass model with roller feet can induce ground reactions, and hence center of mass motion, that emulate normal human walking. The classic inverted pendulum model can be seen as an extreme of the proposed mass-spring model in which the limb stiffness is made very high. An infinitely stiff limb would not absorb energy, leading to the loss of energy seen at heel contact in bipedal inverted pendulum models [3,5]. As a result, an energetic input is required in inverted pendulum models from either a down slope [1] or an impulsive push-off force [4] to maintain a repeatable walking cycle. While this step-to-step energetic demand has been correlated with the metabolic costs associated with walking [5], it is interesting to note that the proposed mass-spring model is able to walk on level ground with no external energy input. This is not to say that the model suggests that humans could walk with zero energy costs since active modulation of muscle stiffness would be needed to maintain the constant limb stiffness. However, this energy expenditure would be distributed throughout the gait cycle, not just occurring at the step-to-step transitions. An additional noteworthy aspect of the proposed mass-spring model is its ability to represent a finite double support period. This is an improvement over compass models, in which step-to-step transitions occur instantaneously.

An improvement of the current mass-spring model over that proposed by Geyer et al. [11] is the incorporation of a roller foot.

We have shown that the roller produces two desirable effects that bring the simulated walking motion closer to that of humans. First the COP naturally progresses from the heel to the toe over the stance phase. We found that a roller radius of 0.3 m resulted in COP excursion that best agreed with experimental data at slow, preferred, and fast walking speeds (Fig. 7). This roller radius is similar to the 30% limb length measured by Hansen et al. [7]. The second important effect of the roller was a reduction in the magnitude of the A-P and vertical ground reaction forces during stance (Fig. 4), which better reflects the magnitude of forces seen in human walking (Fig. 7). The net ground reaction force in our model always points from the current COP to the center of mass of the model. Therefore, a reduction in the peak A-P forces is a natural consequence of allowing the COP to progress.

The model provides insights into possible mechanisms by which walking speed can be modulated. The strategy utilized by the model to facilitate speed variations similar to humans involved the simultaneous modulation of the limb impact angle and limb stiffness. Our simulations were able to closely replicate the COP progression at all speeds and the vertical and A-P ground reactions at the slow and preferred speeds. However, the fast speed solution overestimated the magnitude of braking force during early support and the vertical force oscillation during stance (Fig. 7). This result could reflect two limitations associated with the model. First, while the model is restricted to the sagittal plane motion, it is known that out of plane motion in human walking (i.e., pelvic rotation) contributes to the sagittal center of mass motion and step length [13]. The planar restriction may result in our model utilizing greater impact angles to achieve the experimentally observed step lengths. As mentioned previously, increasing impact angle leads to greater oscillation of the vertical ground reaction force (Fig. 6). Second, during human walking the swing limb retracts during late swing, which would diminish the braking force at heel strike. In contrast, the swing limb of the model is stationary at heel strike, which would contribute to greater braking during the first ~10% of stance (Fig. 7).

One needs to exercise caution when interpreting model vari-

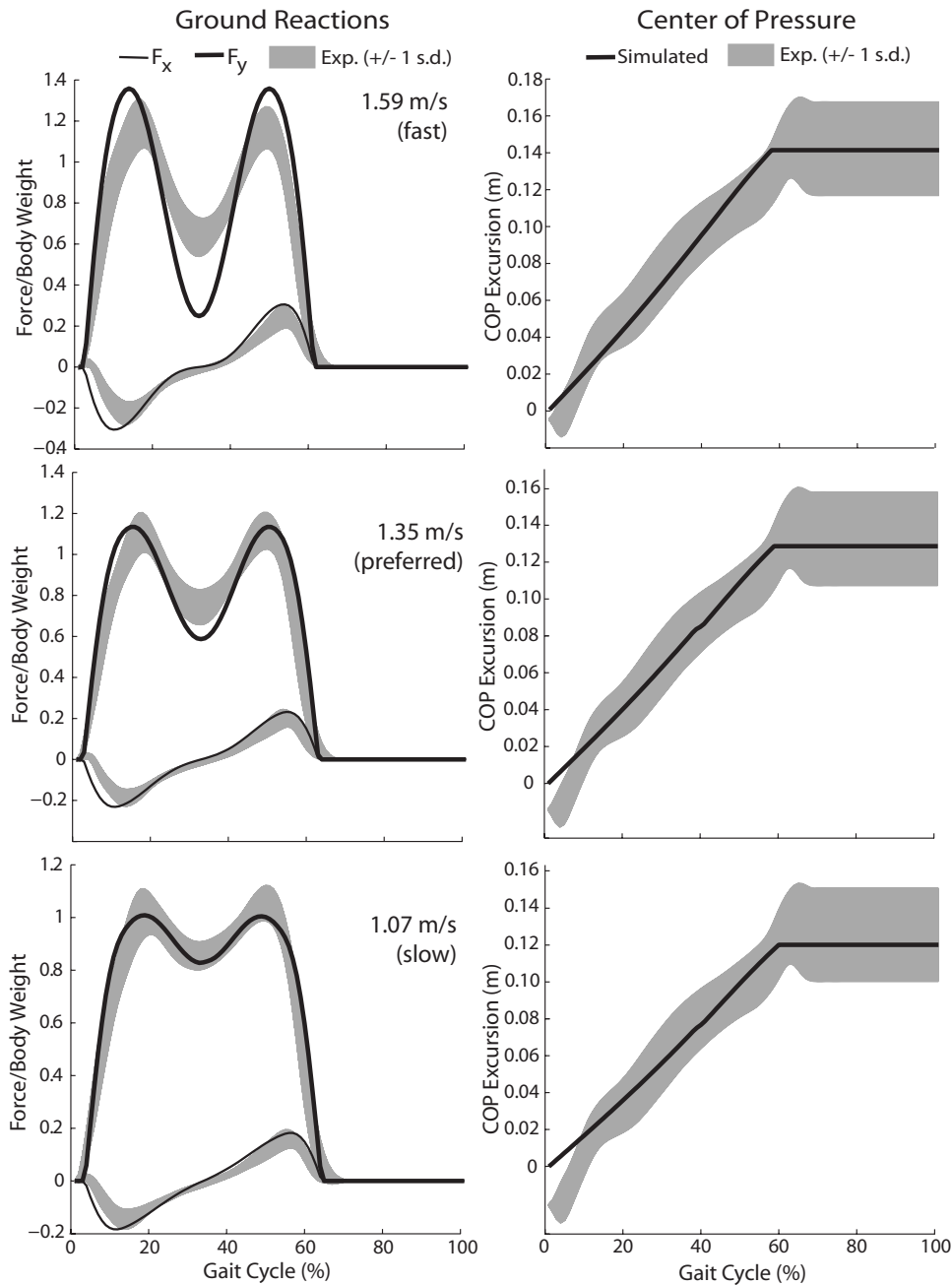


Fig. 7 Use of the model parameters given in Table 1 induced anterior (F_x) and vertical (F_y) ground reaction forces that most closely resembled average experimental (expt) forces at the slow walker speed. At the faster walking speed, the simulated ground reactions exhibited greater variation in stance than seen experimentally. For all speeds, a roller radius of 0.3 m resulted in reasonable approximations of the COP excursion.

Table 1 Given are the model parameters that produced simulations (sim) that were within one standard deviation of the measured step length and cadence and also best replicated the experimental (expt) ground reactions at each walking speed. Differences between the simulated forces and average measurements were quantified by the rms error (expressed as % body weight (%BW)) over a gait cycle

Speed (% preferred)		R (m)	K (N/m)	θ (deg)	Speed (m/s)	Step length (m)	Cadence (steps/s)	rms errors F_x	(%BW) F_y
80	sim	0.3	21,000	23.5	1.07	0.64	1.66	2.8	6.7
	expt				1.06 (± 0.11)	0.66 (± 0.05)	1.62 (± 0.16)		
100	sim	0.3	22,000	25.25	1.35	0.70	1.94	4.1	10.8
	expt				1.35 (± 0.13)	0.74 (± 0.07)	1.83 (± 0.14)		
120	sim	0.3	24,000	27.5	1.59	0.77	2.06	5.5	19.3
	expt				1.59 (± 0.14)	0.81 (± 0.06)	1.96 (± 0.16)		

ables in terms of specific joint variables measured during human walking. For example, the limb (spring) angle in the model does not strictly correspond to the hip joint angle. Instead, the limb angle represents the orientation of a line between the roller center and the whole body center of mass. In human walking, this measure would be a function of pelvic, hip, knee, and ankle joint angles. Similarly, the point mass in the model does not represent the hip center or any other fixed point on the body but rather the whole body center of mass. Further, the model has massless limbs and therefore does not simulate swing phase dynamics. Given the ballistic nature of the swing phase, it is conceivable that this aspect could be added to the model, albeit at the expense of model simplicity.

The proposed mass-spring model of walking has a number of potential uses. First, the simplified model may provide a basis for controlling high degree of freedom walking models [14] and/or bipedal robots [15]. In particular, musculotendon stiffness could be actively modulated to achieve the desired stiffness of the limb and hence the periodic movement pattern that it induces. Doing this would require that the posture-dependent action of muscles be accounted for when reflecting muscle stiffness to limb stiffness. The Jacobian, relating muscle actions to end-point stiffness, could be used to efficiently compute this transformation [16]. Second, spring-mass models [11] have shown the ability to replicate other modes of locomotion such as running. An understanding of the parameters that generate different locomotion patterns could provide a unified framework for understanding gait transitions. A final use of the model would be to characterize an individual's gait pattern using a minimal set of parameters (limb stiffness, impact angle, roller radius, and energy level). The wide range of limit cycle walking solutions achievable by the simple mass-spring model could be exploited in distinguishing variations in human walking patterns. Such parameters could conceivably also be tracked over time, thereby providing a potential mechanism for tracking changes in gait associated with pathology, aging, or clinical interventions.

Acknowledgment

The authors would like to acknowledge Amy Silder and Bryan Heiderscheit for their contributions to walking data collection and processing. This work was supported by NIH Grant No. AG24276.

Nomenclature

M	= point mass
g	= gravitational acceleration
R	= roller radius
K	= limb stiffness
Θ	= limb impact angle
H	= center of mass height in an upright unstretched configuration
TE	= total system energy
L_0	= spring resting length
L_i	= limb length (trailing limb $i=1$; leading limb $i=2$)
θ_i	= limb angle
\dot{L}_i	= limb linear velocity
$\dot{\theta}_i$	= limb angular velocity
\ddot{L}_i	= limb linear acceleration
$\ddot{\theta}_i$	= limb angular acceleration
\vec{v}	= point mass velocity
V	= potential energy
T	= kinetic energy
\mathcal{L}	= Lagrangian

Appendix A: Lagrangian Formulation of Equations of Motion

The equations of motion of the conservative mass-spring model (Fig. 8) were derived using a Lagrangian formulation. The total potential energy, V , in the system includes the elastic energy stored in the springs and the gravitational energy associated with the height of the mass M ,

$$V = \frac{1}{2}K(L_0 - L_1)^2 + \frac{1}{2}K(L_0 - L_2)^2 + (R + L_i \cos \theta_i)Mg \quad (A1)$$

where K represents the spring stiffness, L_0 represents the unstretched spring lengths, L_1 represents the trailing spring length, L_2 represents the leading spring length, R represents the roller radius, M represents the point mass, g is the gravitational constant, and L_i and θ_i refer to a limb currently in contact.

The velocity, \vec{v} , of the point mass M can be conveniently expressed via components directed both perpendicular (\vec{e}_{θ_1}) and parallel (\vec{e}_{L_1}) to the trailing limb,

$$\vec{v} = (L_1 \dot{\theta}_1 + R \dot{\theta}_1 \cos \theta_1) \vec{e}_{\theta_1} + (\dot{L}_1 + R \dot{\theta}_1 \sin \theta_1) \vec{e}_{L_1} \quad (A2)$$

where $\dot{\theta}_1$ represents the angular velocity of the trailing limb. The total kinetic energy, T , in the system is thus given by

$$T = \frac{1}{2}M[(L_1 \dot{\theta}_1 + R \dot{\theta}_1 \cos \theta_1)^2 + (\dot{L}_1 + R \dot{\theta}_1 \sin \theta_1)^2] \quad (A3)$$

The potential and kinetic energy expressions can be combined to form the Lagrangian, $\mathcal{L} = T - V$, of the system, which is a function of the limb lengths (L_1, L_2) and the trailing limb angle θ_1 ,

$$\begin{aligned} \mathcal{L} = & \frac{1}{2}M(L_1^2 \dot{\theta}_1^2 + 2L_1 \dot{\theta}_1^2 R \cos \theta_1 + \dot{L}_1^2 + 2\dot{L}_1 R \dot{\theta}_1 \sin \theta_1 + R^2 \dot{\theta}_1^2) \\ & - MgR + MgL_1 \cos \theta_1 + KL_0^2 - KL_0 L_1 + \frac{1}{2}KL_1^2 - KL_0 L_2 + \frac{1}{2}KL_2^2 \end{aligned} \quad (A4)$$

However, the system possesses only two independent degrees of freedom such that the angular velocity and spring velocity of the leading limb can be described in terms of the respective velocities of the trailing limb (Eq. (2) from text). The Jacobian terms describing incremental changes in L_2 as a function of L_1 and θ_1 can be taken directly from this relationship and are given by

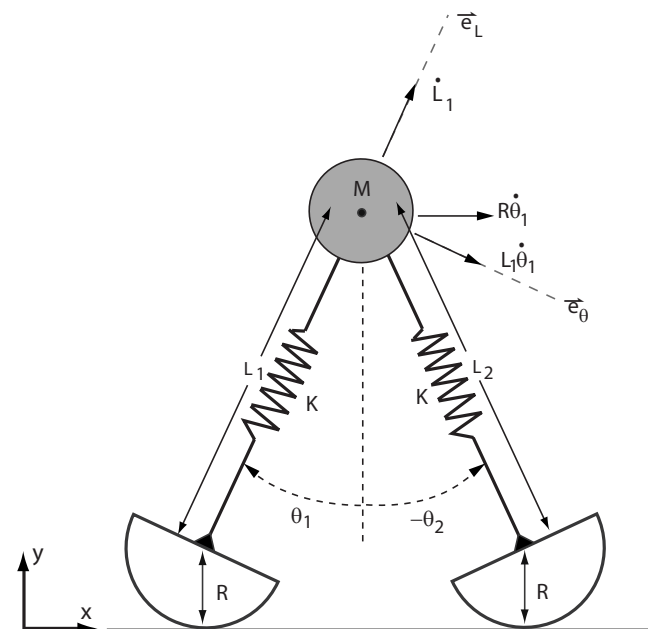


Fig. 8 The velocity of the mass M can be decomposed by components in the forward (x) direction and both along and perpendicular to the trailing limb

$$\frac{\partial L_2}{\partial L_1} = \frac{L_2 \cos(\theta_1 - \theta_2) + R \cos \theta_1}{L_2 + R \cos \theta_2} \quad (\text{A5})$$

$$\frac{\partial L_2}{\partial \theta_1} = \frac{RL_2 \sin \theta_2 - L_1 L_2 \sin(\theta_1 - \theta_2) - RL_1 \sin \theta_1}{L_2 + R \cos \theta_2} \quad (\text{A6})$$

The Lagrangian equations of motion are given by

$$\frac{d}{dt} \left(\frac{\partial \mathcal{L}}{\partial \dot{L}_1} \right) - \left[\frac{\partial \mathcal{L}}{\partial L_1} + \frac{\partial \mathcal{L}}{\partial L_2} \left(\frac{\partial L_2}{\partial L_1} \right) \right] = 0 \quad (\text{A7})$$

$$\frac{d}{dt} \left(\frac{\partial \mathcal{L}}{\partial \dot{\theta}_1} \right) - \left[\frac{\partial \mathcal{L}}{\partial \theta_1} + \frac{\partial \mathcal{L}}{\partial L_2} \left(\frac{\partial L_2}{\partial \theta_1} \right) \right] = 0 \quad (\text{A8})$$

Substituting Eqs. (A4)–(A6) into Eqs. (A7) and (A8) results in the system equations of motion,

$$\begin{aligned} M(\ddot{L}_1 + R\ddot{\theta}_1 \sin \theta_1 + R\dot{\theta}_1^2 \cos \theta_1) - ML_1\ddot{\theta}_1^2 - M\dot{\theta}_1^2 R \cos \theta_1 \\ + Mg \cos \theta_1 - KL_0 + KL_1 - (KL_0 - KL_2) \\ \times \left(\frac{L_2 \cos(\theta_1 - \theta_2) + R \cos \theta_1}{L_2 + R \cos \theta_2} \right) = 0 \end{aligned} \quad (\text{A9})$$

$$\begin{aligned} ML_1^2 \ddot{\theta}_1 + 2ML_1 \dot{\theta}_1 R \cos \theta_1 + MR^2 \ddot{\theta}_1 + M\dot{L}_1 R \sin \theta_1 + 2ML_1 \dot{L}_1 \dot{\theta}_1 \\ + 3M\dot{L}_1 \dot{\theta}_1 R \cos \theta_1 - ML_1 \dot{\theta}_1^2 R \sin \theta_1 - M\dot{L}_1 R \dot{\theta}_1 \cos \theta_1 \\ - Mg L_1 \sin \theta_1 - (KL_0 - KL_2) \\ \times \left(\frac{RL_2 \sin \theta_2 - L_1 L_2 \sin(\theta_1 - \theta_2) - RL_1 \sin \theta_1}{L_2 + R \cos \theta_2} \right) = 0 \end{aligned} \quad (\text{A10})$$

The equations can then be rewritten in matrix form as a pair of coupled nonlinear second order differential equations (see Eq. (1)). These two equations of motion are sufficient to describe the dynamics during both single and double supports. During the single support phase, the massless noncontact limb is set to the limb impact angle and maintained there. During the double support phase, the closed loop kinematic coupling allows for the motion of the leading limb to be computed given the positions, velocities, and acceleration of the trailing limb (see Eqs. (2) and (3)).

Appendix B: Calculation of Ground Reaction Force

The vertical and A-P ground reaction forces attributable to each limb can be calculated by recognizing that the line of action of each limb force points from the COP to the center of mass (Fig. 9). Thus, the angle of the ground force vector, ϕ , for each limb is given by

$$\phi = \tan^{-1} \left(\frac{L \sin \theta}{R + L \cos \theta} \right) \quad (\text{B1})$$

The component of the ground reaction force vector acting along the limb spring, F_L , is simply the spring force,

$$F_L = K(L_0 - L) \quad (\text{B2})$$

Knowing F_L and the ground force vector direction, the force perpendicular to the limb spring, F_θ , can then be determined,

$$F_\theta = -F_L \tan(\theta - \phi) \quad (\text{B3})$$

The forces F_L and F_θ are then transformed into the ground reference frame to determine the forces acting in the fore-aft (F_x) and vertical (F_y) directions,

$$F_x = \sqrt{F_L^2 + F_\theta^2} \sin(\phi) \quad (\text{B4})$$

$$F_y = \sqrt{F_L^2 + F_\theta^2} \cos(\phi) \quad (\text{B5})$$

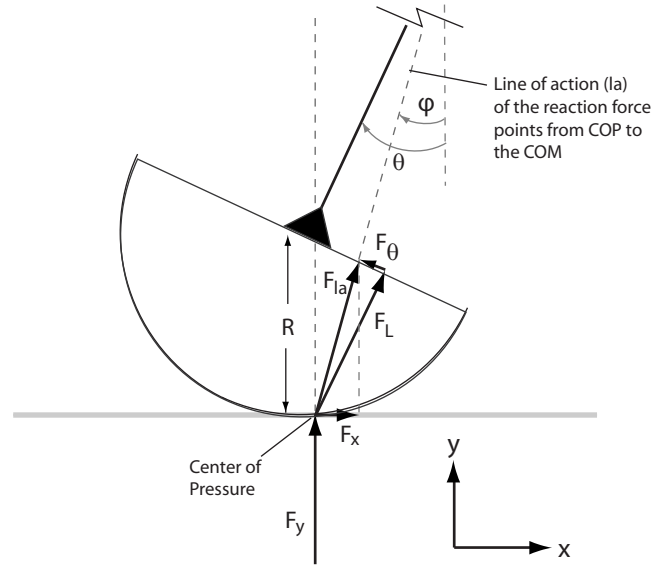


Fig. 9 The ground reaction force vectors F_x and F_y for each limb are computed knowing the spring force F_L and the angle ϕ that the ground reaction force vector forms with the vertical

References

- [1] McGeer, T., 1990, "Passive Dynamic Walking," *Int. J. Robot. Res.*, **9**(2), pp. 62–82.
- [2] Cavagna, G. A., Thys, H., and Zamboni, A., 1976, "The Sources of External Work in Level Walking and Running," *J. Physiol. (London)*, **262**(3), pp. 639–657.
- [3] Garcia, M., Chatterjee, A., Ruina, A., and Coleman, M., 1998, "The Simplest Walking Model: Stability, Complexity, and Scaling," *ASME J. Biomech. Eng.*, **120**(2), pp. 281–288.
- [4] Kuo, A. D., 2002, "Energetics of Actively Powered Locomotion Using the Simplest Walking Model," *ASME J. Biomech. Eng.*, **124**(1), pp. 113–120.
- [5] Kuo, A. D., Donelan, J. M., and Ruina, A., 2005, "Energetic Consequences of Walking Like an Inverted Pendulum: Step-to-Step Transitions," *Exerc Sport Sci. Rev.*, **33**(2), pp. 88–97.
- [6] Adamczyk, P. G., Collins, S. H., and Kuo, A. D., 2006, "The Advantages of a Rolling Foot in Human Walking," *J. Exp. Biol.*, **209**, pp. 3953–3963.
- [7] Hansen, A. H., Childress, D. S., and Knox, E. H., 2004, "Roll-Over Shapes of Human Locomotor Systems: Effects of Walking Speed," *Clin. Biomech. (Bristol, Avon)*, **19**(4), pp. 407–414.
- [8] Buczek, F. L., Cooney, K. M., Walker, M. R., Rainbow, M. J., Concha, M. C., and Sanders, J. O., 2006, "Performance of an Inverted Pendulum Model Directly Applied to Normal Human Gait," *Clin. Biomech. (Bristol, Avon)*, **21**(3), pp. 288–296.
- [9] Mochon, S., and McMahon, T. A., 1980, "Ballistic Walking," *J. Biomech.*, **13**, pp. 49–57.
- [10] McMahon, T. A., and Cheng, G. C., 1990, "The Mechanics of Running: How Does Stiffness Couple With Speed?," *J. Biomech.*, **23**, pp. 65–78.
- [11] Geyer, H., Seyfarth, A., and Blickhan, R., 2006, "Compliant Leg Behaviour Explains Basic Dynamics of Walking and Running," *Proc. R. Soc. London, Ser. B*, **273**(1603), pp. 2861–2867.
- [12] Geyer, H., Seyfarth, A., and Blickhan, R., 2005, "Spring-Mass Running: Simple Approximate Solution and Application to Gait Stability," *J. Theor. Biol.*, **232**(3), pp. 315–328.
- [13] Kerrigan, D. C., Riley, P. O., Lelas, J. L., and Della Croce, U., 2001, "Quantification of Pelvic Rotation as a Determinant of Gait," *Arch. Phys. Med. Rehabil.*, **82**(2), pp. 217–220.
- [14] Delp, S. L., Loan, J. P., Hoy, M. G., Zajac, F. E., Topp, E. L., and Rosen, J. M., 1990, "An Interactive Graphics-Based Model of the Lower Extremity to Study Orthopaedic Surgical Procedures," *IEEE Trans. Biomed. Eng.*, **37**(8), pp. 757–767.
- [15] Collins, S., Ruina, A., Tedrake, R., and Wisse, M., 2005, "Efficient Bipedal Robots Based on Passive-Dynamic Walkers," *Science*, **307**(5712), pp. 1082–1085.
- [16] Hogan, N., 1990, "Mechanical Impedance of Single- and Multi-Articular Systems," *Multiple Muscle Systems: Biomechanics and Movement Organization*, J. M. Winters and S. L.-Y. Woo, eds., Springer-Verlag, New York, pp. 149–164.